Water Contaminant Mitigation in Ionic Liquid Propellant

IEPC-2009-172

Presented at the 31st International Electric Propulsion Conference,
University of Michigan • Ann Arbor, Michigan • USA
September 20 – 24, 2009

Dr. David Conroy[1], Dr. John Ziemer[2]
Jet Propulsion Laboratory, Pasadena, CA, 91109-8099

Abstract: Appropriate system and operational requirements are needed in order to ensure mission success without unnecessary cost. Purity requirements applied to thruster propellants may flow down to materials and operations as well as the propellant preparation itself. Colloid electrospray thrusters function by applying a large potential to a room temperature liquid propellant (such as an ionic liquid), inducing formation of a Taylor cone. Ions and droplets are ejected from the Taylor cone and accelerated through a strong electric field. Electrospray thrusters are highly efficient, precise, scaleable, and demonstrate low thrust noise. Ionic liquid propellants have excellent properties for use as electrospray propellants, but can be hampered by impurities, owing to their solvent capabilities. Of foremost concern is the water content, which can result from exposure to atmosphere. Even hydrophobic ionic liquids have been shown to absorb water from the air. In order to mitigate the risks of bubble formation in feed systems caused by water content of the ionic liquid propellant, physical properties of the ionic liquid EMI–Im are analyzed. The effects of surface tension, material wetting, physisorption, and geometric details of the flow manifold and electrospray emitters are explored. Results are compared to laboratory test data.

I. Introduction

Appropriate system and operational requirements are needed in order to ensure mission success without unnecessary cost. Proper requirements formulation and compliance will prevent the formation of gas bubbles in the propellant, which carries risks of degradation of thruster response times or subsystem failure if not mitigated. In operation, bubbles introduce compressibility in the feed system, which adversely effects response time to throttling commands. If there is no forced flow, the resulting low pressure allows bubbles to grow, which carries the risk of forcing conductive propellant out until it bridges the gap between the emitter and the extractor electrode.

The ST7 disturbance reduction system (DRS) system was plagued by the effects of bubbles in the feed system in early development. Empirically, it was found that initial concentrations of water in the propellant of 150 ppm or below resulted in well behaved DRS system performance.

The goals of this work are: 1, to increase the confidence of the established ST7 requirement through a deeper understanding of the physical processes taking place in bubble formation, evolution, and transport within the propellant feed manifold, and 2, to use this same knowledge to provide technical reasoning for the application or modification of this requirement for the LISA DRS system.

In order to analyze the impact of the existence of a bubble in the propellant manifold, the contributions to manifold pressure of surface tension by the meniscus at the emitter and that of the bubble surface itself are compared to the propellant mixture's vapor pressure. All these values are functions of water content and temperature. Published work on the propellant properties does not cover the regime of the LISA system's environmental requirements, and the literature results were therefore extended using a combination of molecular statistical mechanics models and further experimental measurements.

[1] Research Scientist, Analytical Chemistry and Materials Development Group, john.k.ziemer@jpl.nasa.gov.
[2] Senior Engineer, Electric Propulsion Group, john.k.ziemer@jpl.nasa.gov.

The initial water content of the propellant is presumed to increase due to atmospheric water adsorbed onto the wetted surfaces of the feed system. The effect of this adsorbed water may be estimated from internal areas and cleanliness of the manifold, and applied retroactively to the vapor pressure findings in order to establish an initial water content requirement.

A resultant propellant water content requirement of 150 ppm is derived for the LISA project, which matches previous experience during development of the ST7 DRS.

II. Water Contamination in EMI–Im

EMI–Im is an ionic liquid, a room temperature mixture composed of positively charged cations and negatively charged anions. Low viscosity, high conductivity, and negligible vapor pressure make it a desirable colloid thruster propellant. Impurities in the EMI–Im, notably water, can modify these characteristics, degrading performance.

EMI–Im has a molecular weight of 391.3 amu. EMI (shorthand for 1-ethyl-3-methylimidazolium) is the cation (+), with a molecular weight of 111.2 amu. Im (bis trifluoromethylsulfonyl imide) is the partner anion (–), with a molecular weight of 280.2 amu.

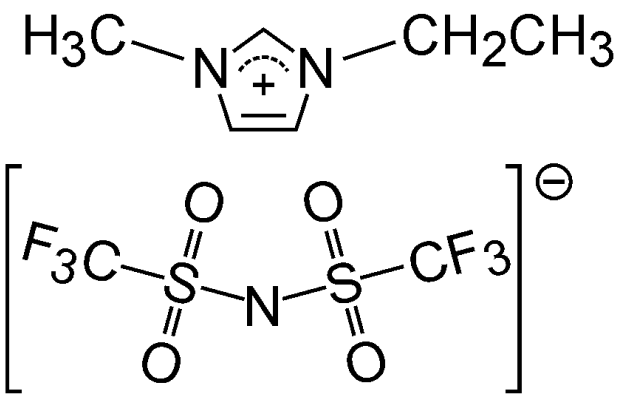

Figure 1. Molecular structure of EMI^+ and Im^- ions.

EMI consists of a five member heteronuclear imidazole ring with methyl and ethyl saturated organic groups bound to the two nitrogen ring members. The positive charge is delocalized among the N–C–N ring members, which renders the hydrogen on the intermediate carbon atom acidic. Im has two sulfonyl groups bound to a central nitrogen atom, and a fluorinated methyl group at each end. The negative charge is delocalized among the nitrogen and oxygen atoms, as evidenced by calculations of the molecular bond lengths of the anion compared to the analogous neutral.[1]

When left under typical Earth ambient conditions, EMI–Im will absorb water from the air. Once subjected to vacuum, this can lead to water gas evolution from the mixture to form a bubble, which displaces propellant inside the feed system, and may impede proper propellant flow or lead to a critical short between the emitters and the extractor electrode. Controlling the amount of water content of the propellant is important for prevention of DRS failure, and understanding the phase behavior of the binary mixture in the context of the feed system is important for establishing the degree of control required.

A. Vapor Pressure of Water in EMI–Im

The vapor pressure above an ideal solution conforms to Raoult's Law, which states that the partial pressure of each substituent above the mixture is equal to the mole fraction of that substituent in the solution multiplied by the vapor pressure of the pure substance. The vapor pressure of an ideally dilute solution conforms to Henry's Law, which is similar except that the vapor pressure term is multiplied by an "activity coefficient."

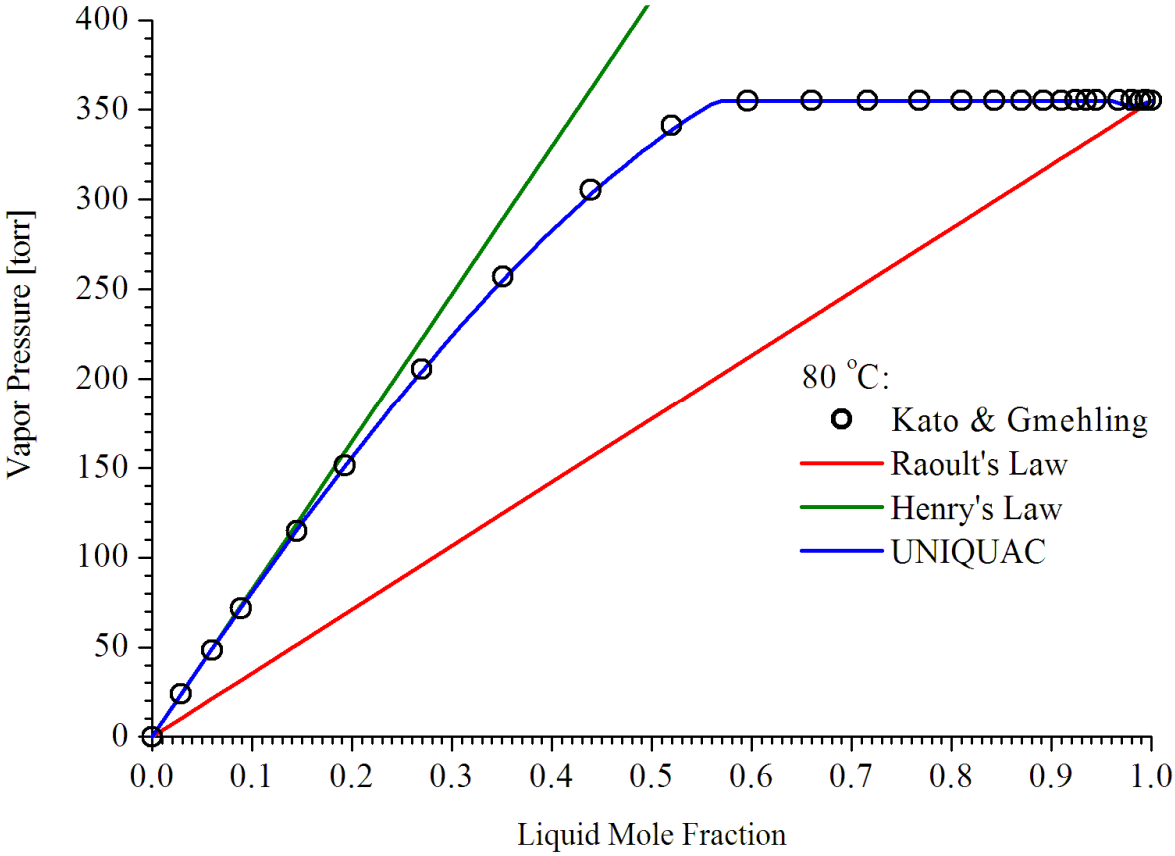

Figure 2 Vapor pressure of water in a binary mixture with EMI–Im at 80 °C. *Circles show values from vapor pressure measurements, while lines represent predictions using models.*

Measurement of the vapor pressure of water as a function of the binary mixture concentration with EMI–Im was performed by Kato & Gmehling[2] at 80 °C. Figure 2 compares their results with Raoult's Law, clearly showing that EMI–Im is far from an ideal solution. Raoult's Law underestimates the vapor pressures by more than a factor of 2 at the low concentrations of interest. Henry's Law, using the infinitely dilute activity coefficient of 2.32 derived by Kato & Gmehling,[2] overpredicts the vapor pressure to higher degrees as water concentration increases, but is fairly close up to about 5% molar fraction (~2500 ppm). Further determinations of the activity coefficient of water at the limit of infinite dilution in EMI–Im at several temperatures was reported by Krummen, et al.[3]

For prediction of the vapor pressure of water in EMI–Im as a combined function of both molar fraction and temperature in this work, the mixture dependent activity coefficients were computed from the UNIQUAC statistical mechanics model of Abrams & Prausnitz.[4] UNIQUAC parameters for EMI–Im and water were taken from Kato & Gmehling,[2] which shows a reasonable fit to their vapor pressure data at 80 °C.

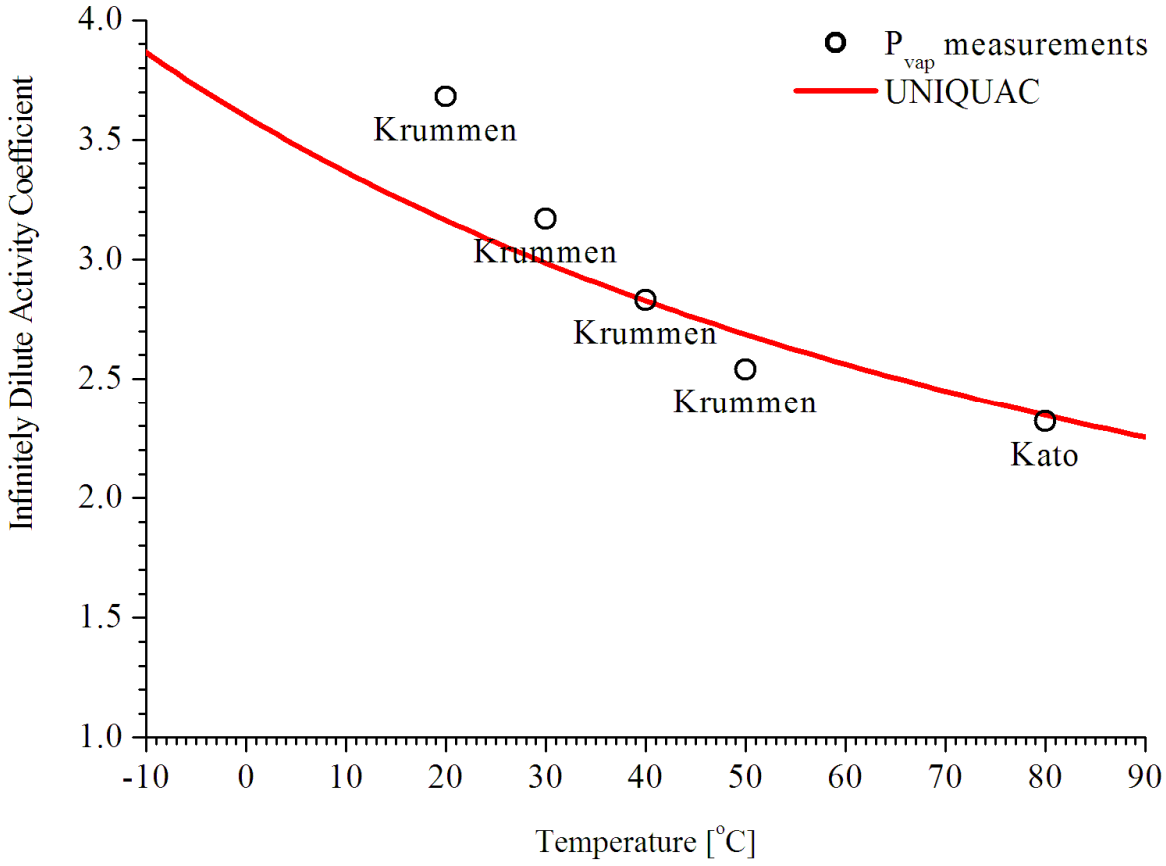

Figure 3. Activity coefficient of water in an infinitely dilute binary mixture with EMI–Im. *Circles show values calculated from vapor pressure measurements, while the red line represents a prediction from the UNIQUAC model.*

Predicted activity coefficients at the limit of zero water content are compared to the infinitely dilute values versus temperature from the literature in Figure 3. The UNIQUAC model draws a reasonable curve through the whole body of available data, although it does not reproduce the trend seen in the Krummen data.

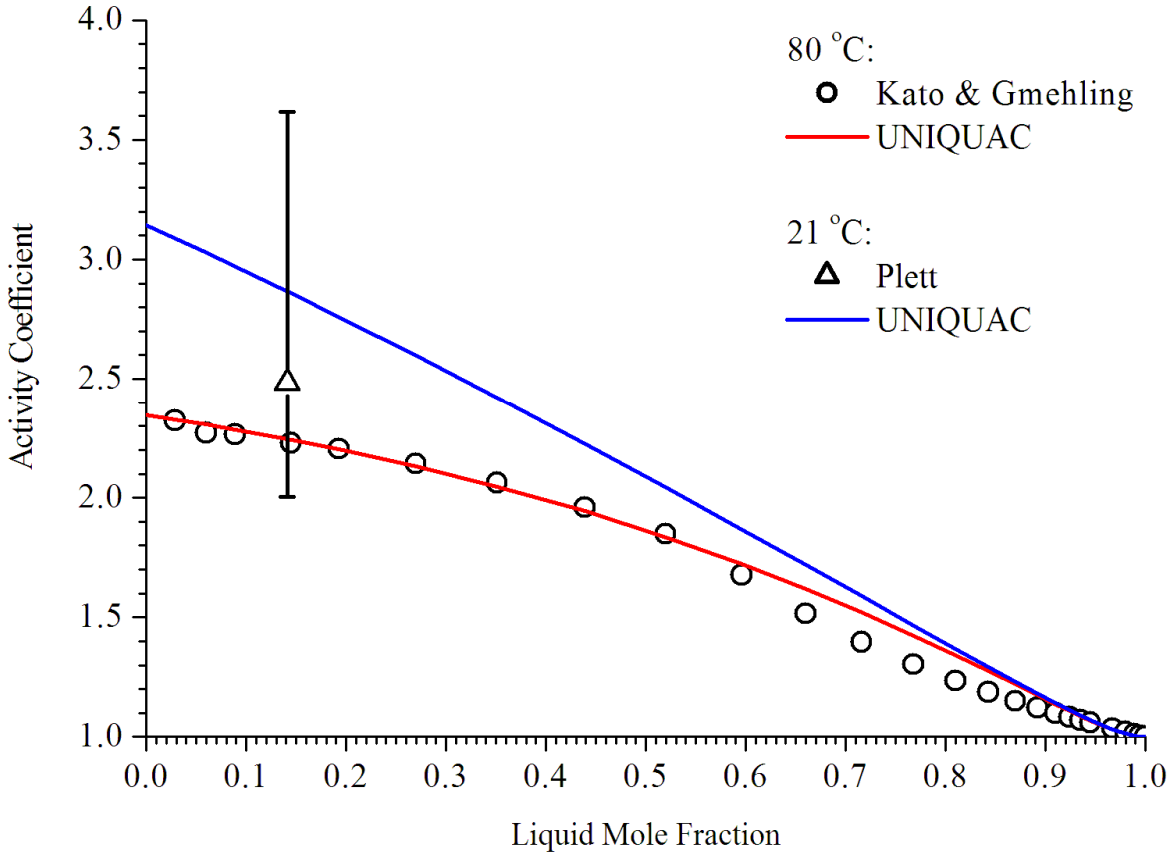

Figure 4. Activity coefficient of varying concentration of water in binary mixture with EMI–Im. *Circles show values calculated from vapor pressure measurements, the triangle represents the value determined from water uptake, and lines represent predictions using the UNIQUAC model.*

Figure 4 displays the Kato & Gmehling activity coefficients versus water content at 80 ºC, as well as an activity coefficient derived from a measurement of water uptake under ambient humidity at room temperature conducted by Gary Plett at the Jet Propulsion Laboratory. The large error bars delineate the extrema of variations in ambient conditions (35% ± 5% relative humidity, 21 ºC ± 1 ºC temperature) during the duration of the test. Both cases are compared to the UNIQUAC model.

B. Surface tension of a mixture of EMI–Im with Water

Consider a simple model of bubble expansion inside a manifold with large volume (and thus a constant supply of water impurity) and emitters that have a chamfered exit termination leading to an ambient vacuum. With the propellant flow system quiescent, bubbles inside the manifold experience no resistance to expansion until propellant is forced to the tips of the emitters and forms a convex meniscus there. Surface tension at the meniscus causes a pressure increase in the propellant mixture, according to Equation 1.

$$\Delta P = \gamma \frac{\partial A}{\partial V} \tag{1}$$

Where γ is the surface tension, and $\partial A/\partial V$ is the ratio of surface area change to volume change.

The geometry of a droplet formed outside the emitter tip, with a spherical surface of radius of curvature r, and a constant wetted area (radius h) spanning the outside diameter of the emitter tip, is shown in Figure 5. Integration of the differential surface area and volume along ℓ yields A and V, as shown in Equations 2 and 3. The differential with respect to r of each of these leads to a simple expression for $\partial A/\partial V$ as shown in Equation 4. This result is identical to that of a full spherical bubble.

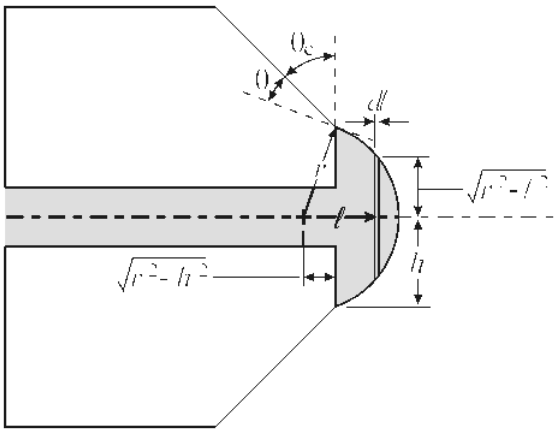

Figure 5. Initial geometry of a model droplet formed at the tip of the emitter.

$$V = \int_{\sqrt{r^2-h^2}}^{r} \pi\left(r^2 - \ell^2\right)\cdot \partial\ell = \pi\left\{\frac{2}{3}r^3 \mp r^2\sqrt{r^2-h^2} \pm \frac{\left[r^2-h^2\right]^{\frac{3}{2}}}{3}\right\} \tag{2}$$

$$A = \int_{\sqrt{r^2-h^2}}^{r}\int_0^{2\pi} r\cdot\partial\ell = 2\pi\left\{r^2 \mp r\sqrt{r^2-h^2}\right\} \tag{3}$$

$$\frac{\partial A}{\partial V} = \frac{2\left\{2r - \dfrac{2r^2-h^2}{\sqrt{r^2-h^2}}\right\}}{2r^2 - r\dfrac{3r^2-2h^2}{\sqrt{r^2-h^2}} + r\sqrt{r^2-h^2}} = \frac{2}{r}\cdot\frac{\dfrac{2r\sqrt{r^2-h^2}-2r^2+h^2}{\sqrt{r^2-h^2}}}{\dfrac{2r\sqrt{r^2-h^2}-3r^2+2h^2+r^2-h^2}{\sqrt{r^2-h^2}}} = \frac{2}{r}\cdot\frac{2r\sqrt{r^2-h^2}-2r^2+h^2}{2r\sqrt{r^2-h^2}-2r^2+h^2}$$

$$\frac{\partial A}{\partial V} = \frac{2}{r} \tag{4}$$

The sum of the chamfer angle θ_e and the angle θ between the chamfer and the droplet edge is half of the angular extent of the droplet. Therefore, $\theta_e + \theta$ may be referred to as the "half angle."

/

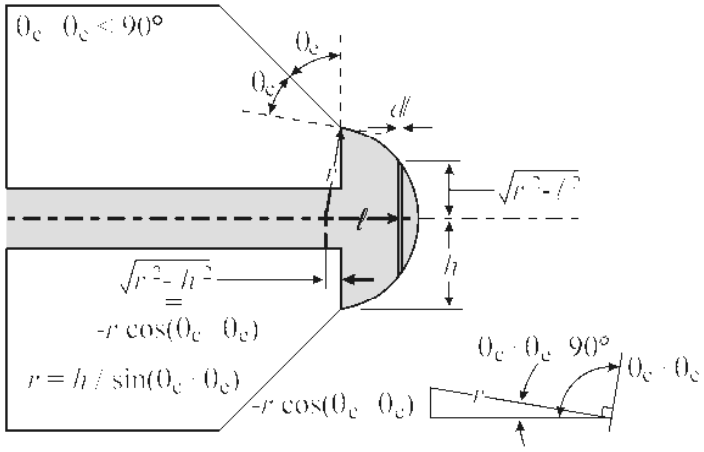

Figure 6. Geometry of the droplet at minimum radius, $\theta_c+\theta_e < 90^o$ case.

As the droplet expands, the radius of curvature reduces, resulting in a meniscus pressure increase. This continues until the extruded propellant forms 1) a hemisphere, or 2) a maximum angle θ with the chamfered surface greater than or equal to the wetting angle θ_c of the propellant with the emitter material, as illustrated in Figure 6. Conventionally, wetting angles are measured on a flat surface. The curvature of the emitter's chamfered surface in the azimuthal direction affects the wetting angle in the axial – radial plane because of the energy minimization intrinsic to the wetting process. For the case of wetting angles less than 90º, the actual angle measured in the axial – radial plane will be perturbed to a larger angle. At the current level of accuracy considered in this work, the conventional wetting angle is used as a minimum value because it provides a minimum meniscus pressure case.

If the maximum half angle is less than 90º, then the droplet is less than a hemisphere, as pictured in Figure 6, and this is the point at which the meniscus radius is at its minimum. Any added volume will cause the droplet to wet the chamfer surface, and the radius of curvature will increase. The geometry of the minimum radius droplet relates the radius to the outer diameter of the very tip of the emitter, which yields an expression for the maximum meniscus pressure given in Equation 5.

$$\Delta P = \frac{2\gamma}{h}\sin\left(\theta_c + \theta_e\right) \tag{5}$$

In the case where $\theta_c + \theta_e \geq 90^o$, the point of minimum radius (and, thus, maximum meniscus pressure) is reached when the droplet has formed a hemisphere, whereupon its center of curvature is coplanar with the emitter tip and its diameter equals the unchamfered tip diameter. In this case, the meniscus pressure is simply that of a spherical bubble of the same diameter as the wetted surface, as shown in Equation 6.

$$\Delta P = \frac{2\gamma}{h} \tag{6}$$

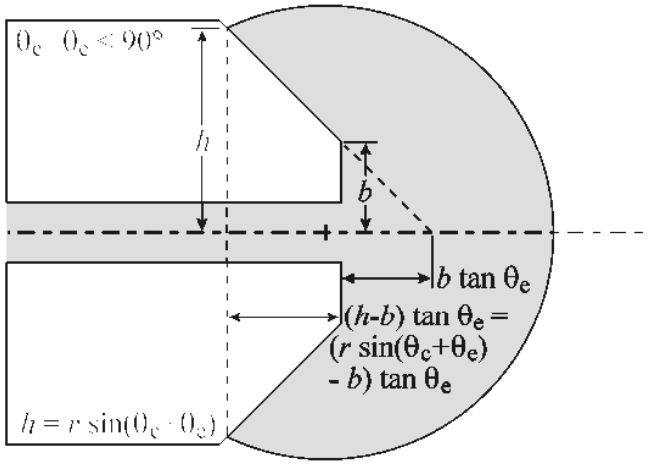

Figure 7. Geometry of the droplet wetting the chamfer, $\theta_c+\theta_e <$ 90º case.

Once the droplet begins to wet the chamfered surface, the volume of the droplet is complicated by the missing volume of the emitter in the shape of a frustrum of a cone, as illustrated in Figure 7 and quantified in Equation 7.

Therefore, the expression describing the meniscus pressure is of the form shown in Equation 8.

$$V = \pi\left\{\frac{2}{3}r^3 \mp r^2\sqrt{r^2-h^2} \pm \frac{\left[r^2-h^2\right]^{\frac{3}{2}}}{3} - \frac{1}{3}\left[r^3\sin^3\left(\theta_c+\theta_e\right) - b^3\right]\tan\theta_e\right\} \tag{7}$$

$$\Delta P = \frac{2\gamma}{r}\cdot\frac{\left[1\mp\cos\left(\theta_c+\theta_e\right)\right]^2}{\left[1\mp\cos\left(\theta_c+\theta_e\right)\right]^2 - \frac{1}{2}\sin^3\left(\theta_c+\theta_e\right)\cos\left(\theta_c+\theta_e\right)\tan\theta_e} \tag{8}$$

Figure 8. Emitter with propellant.

A photo of an actual emitter tip is shown in Figure 8. The pressure exerted on the propellant manifold by the meniscus at the emitter tip serves as the only check on bubble growth when there is no forced flow. At equilibrium, the bubble's internal pressure would be equal to the vapor pressure of the liquid, in this case the vapor pressure of water in the mix. If this pressure exceeds the surrounding pressure, the bubble will expand. Though there is pressure exerted on the bubble by the surface tension of its own walls, it might be very small in the case of a large bubble, and is neglected here. Conditions must be maintained such that the vapor pressure of the propellant is lower than the maximum meniscus pressure of the emitters, or bubble growth may proceed unchecked.

Surface tension measurements of a mixture of 1090 ppm water in EMI–Im was reported by Kilaru et al,[5] evincing a linear dependence on temperature. In the present analysis, the values for 1090 ppm were extended to other mixture ratios using the CRC values for pure water[6] and the surface tension mixing rule of Equation 9.[7] This is an ad hoc estimation, but the effect of water concentration on the surface tension is seen to be minor in the overall analysis.

$$\frac{1}{\sigma} = \frac{\sum_i \frac{n_i}{\sigma_i}}{\sum_i n_i} \tag{9}$$

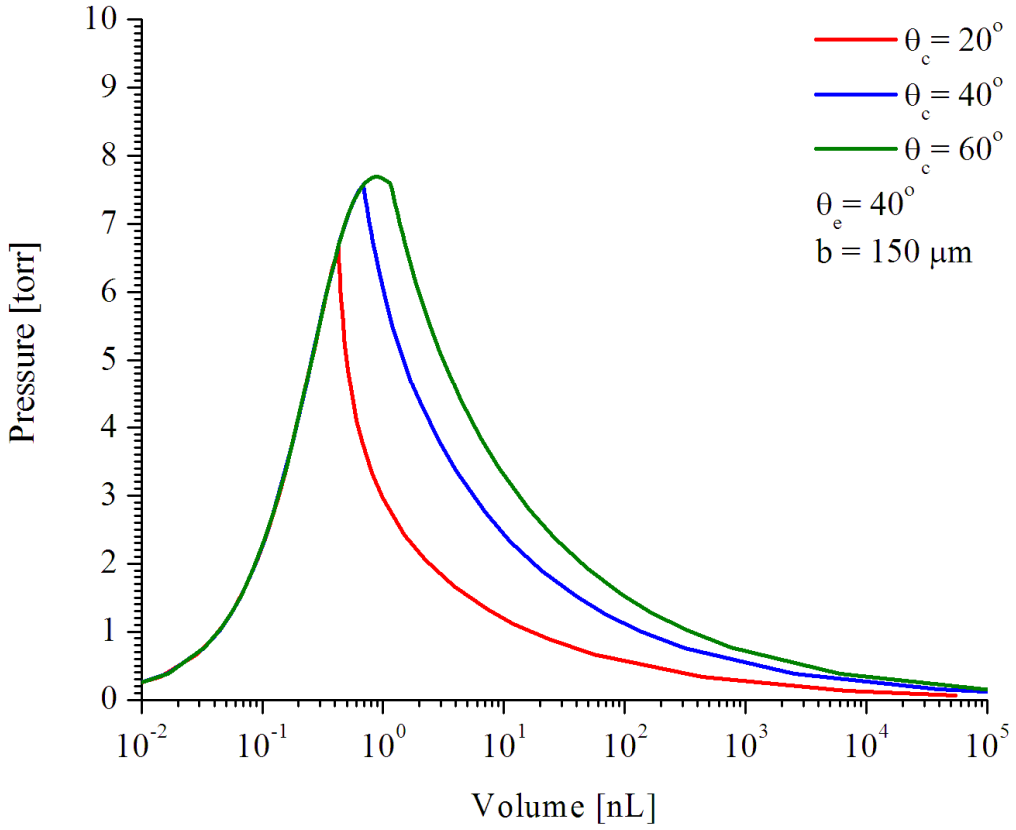

Figure 9. **Model meniscus pressure as a function of droplet volume for different wetting angles.**

Figure 9 shows meniscus pressure plotted vs. *V* at 80 ºC for three different contact angles. A wide range of wetting angles from 20º to 60º were used, since there is so little data for wetting angles of the propellant on materials at this time. It can be seen how the wetting angle influences the maximum pressure resulting from surface tension.

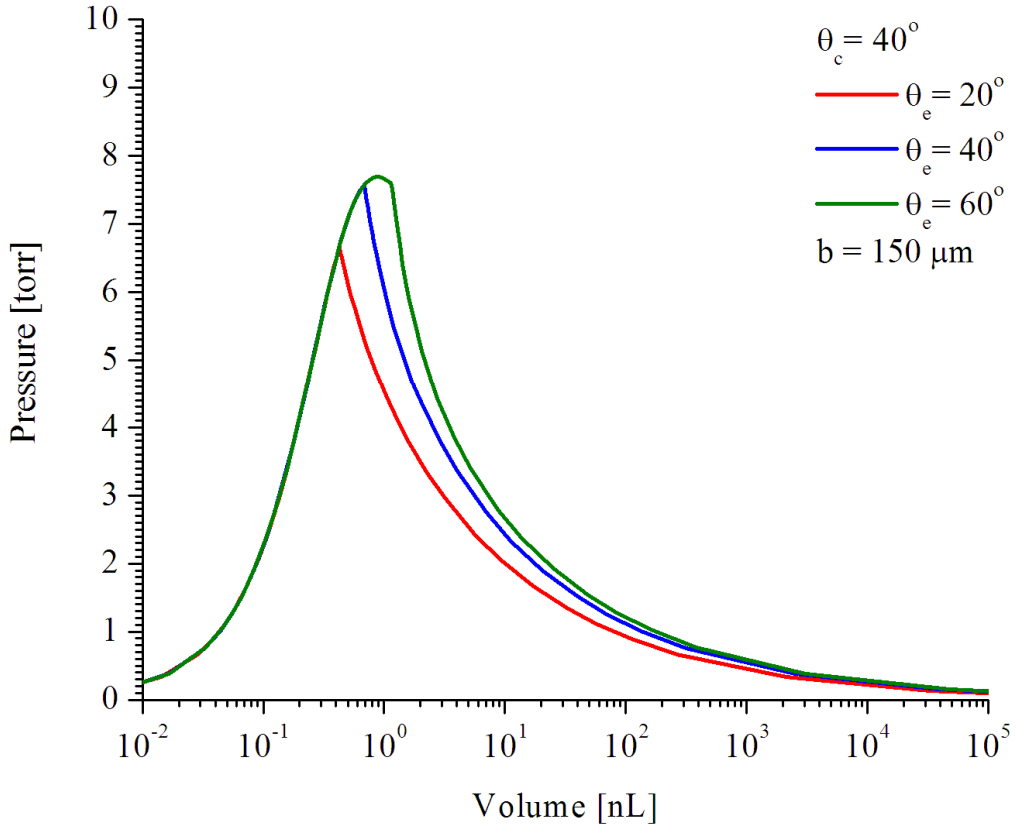

Figure 10. **Model meniscus pressure as a function of droplet volume for different chamfer angles.**

Figure 10 shows the effect of emitter tip chamfer angle on maximum meniscus pressure for an assumed propellant wetting angle of 40º. The higher the degree of chamfer of the emitter, the smaller the minimum radius the extruded propellant droplet is allowed to reach before being forced to wet the chamfer surface, resulting in a higher maximum pressure. This effect is enhanced if the propellant wetting angle is smaller.x

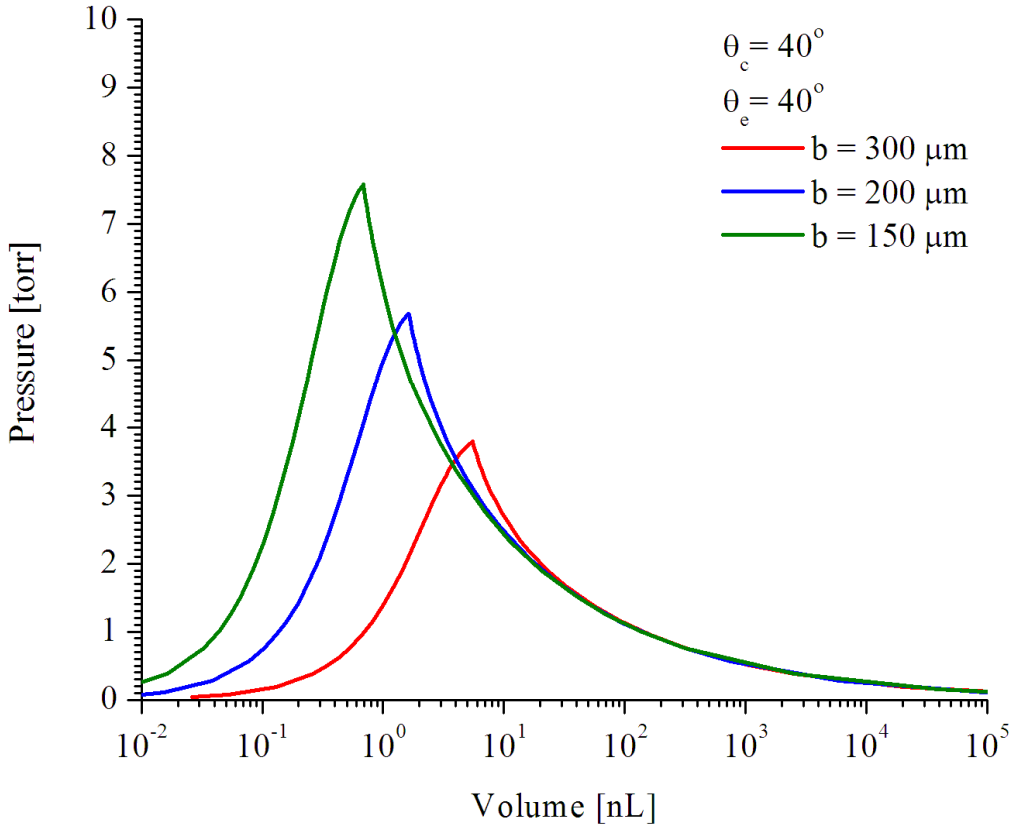

Figure 11. Model meniscus pressure as a function of droplet volume for different emitter flat diameters.

Figure 11 shows the effect of emitter tip diameter on maximum meniscus pressure. The smaller the outside diameter of the flat tip of the emitter, the smaller the minimum radius of the extruded propellant droplet, resulting in a higher maximum pressure.

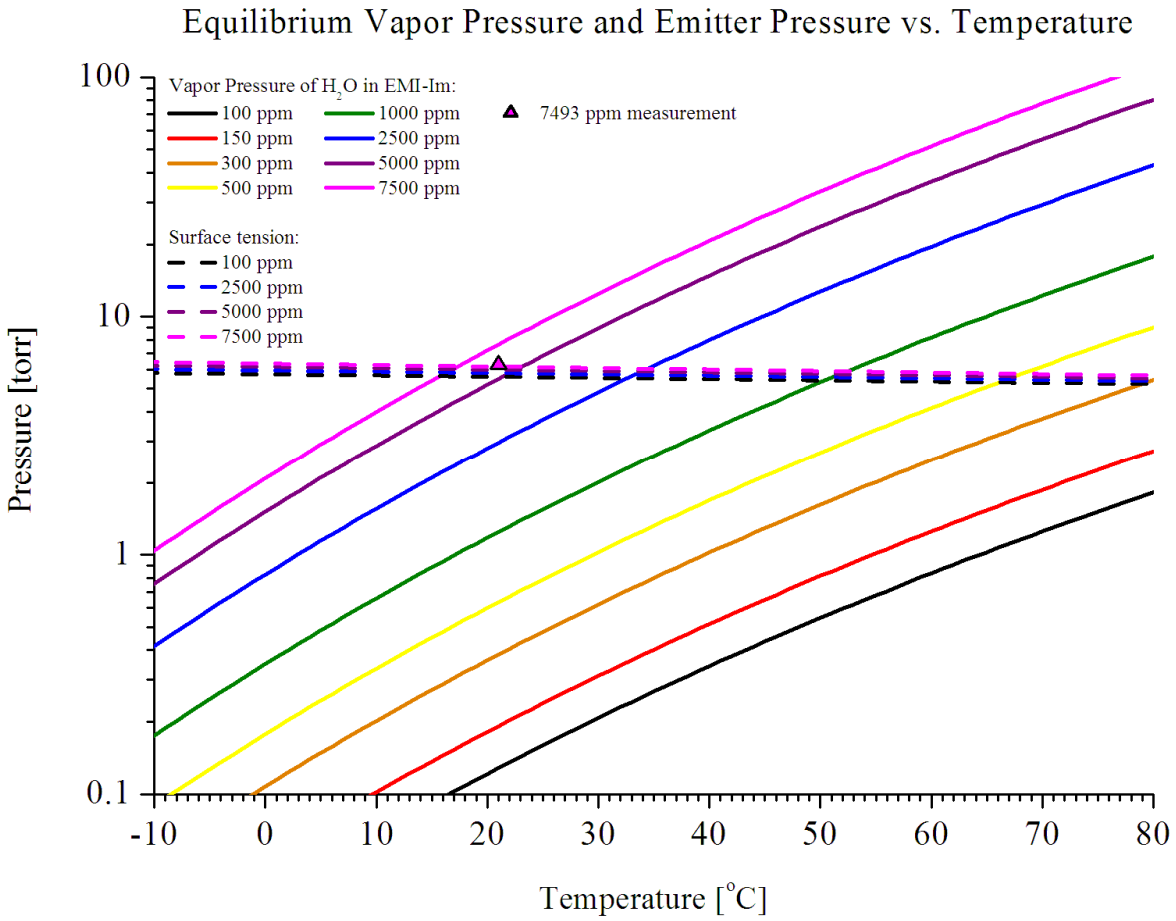

Figure 12. Vapor pressure of water from a binary mixture with EMI–Im at a variety of concentrations compared to maximum meniscus pressure caused by surface tension of propellant outside the emitter tips at several concentrations. *Bubble growth is limited when the vapor pressure is less than the maximum meniscus pressure.*

Figure 12 shows the predicted vapor pressures of a variety of mixture ratios vs temperature as solid curves, along with the maximum predicted meniscus pressures caused by surface tension at the emitter tips as dashed lines. Note how slightly the meniscus pressure depends on the water content, as illustrated by the nearly overlapping lines. In order to avoid unlimited expansion of bubbles inside the manifold, the vapor pressure must be below the corresponding meniscus pressure. For non-operational temperatures up to 60 ºC, the qualifying mixtures in the set are 100, 150, 300, and 500 ppm. For a higher temperature of 80 ºC, 150 ppm would be the maximum water content allowable.

C. Bubble Growth

In order to grow, a bubble's internal pressure must exceed the external pressure. In addition to the meniscus pressure, which acts on the bubble through the bulk propellant, the surface tension of the bubble's own periphery must be overcome by the gas pressure inside the bubble, which is assumed to be equal to the vapor pressure of water in EMI–Im. Figures 13 and 14 illustrate the growth potential of bubbles by plotting the difference in the respective equilibrium pressures (internal – external) as a function of the bubble radius at room and elevated temperatures for a system comprising nine emitters, using dimensions representative of the ST7 flow manifold and an artificially assumed propellant – emitter wetting angle of 20º Computation proceeded from an initial bubble volume of 10 nL and progressed until the wetted area of the emitters exceeded the chamfered surface.

At the very smallest sizes, a bubble is unable to overcome its own surface tension, so the potential for growth is negative and a bubble that size would collapse. Bubbles above the formation threshold exist in the regime of positive potential until they grow large enough to push propellant to the emitter tips, whereupon the meniscus

pressure quickly comes into play and may prevent further growth, as in the case of the 1000 ppm and 2500 ppm mixes at 25 ºC, as well as the 100 ppm and 150 ppm propellant mixes at 80 ºC. Once this hurdle is exceeded, bubble growth is limited only by the amount of water available in the propellant.

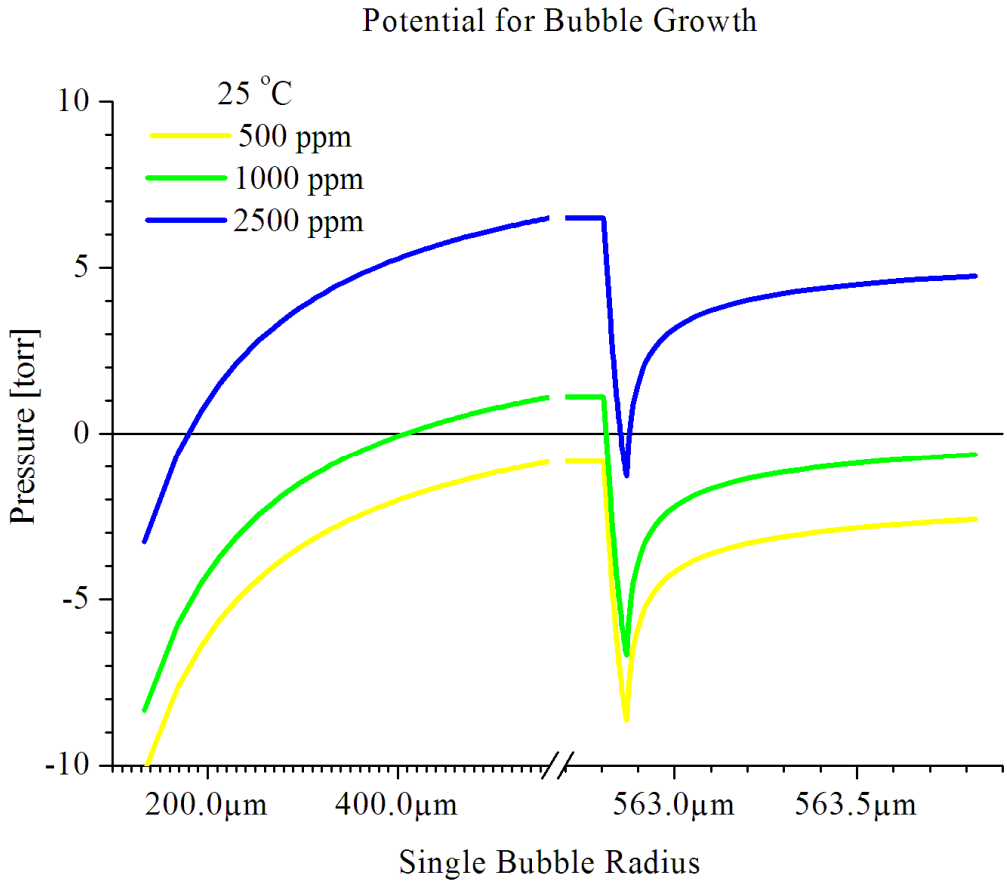

Figure 13. Potential for bubble growth expressed as a difference in equilibrium pressures (vapor pressure – bubble surface tension pressure – meniscus pressure) vs. bubble radius for several concentrations of water in EMI–Im at 25 ºC.

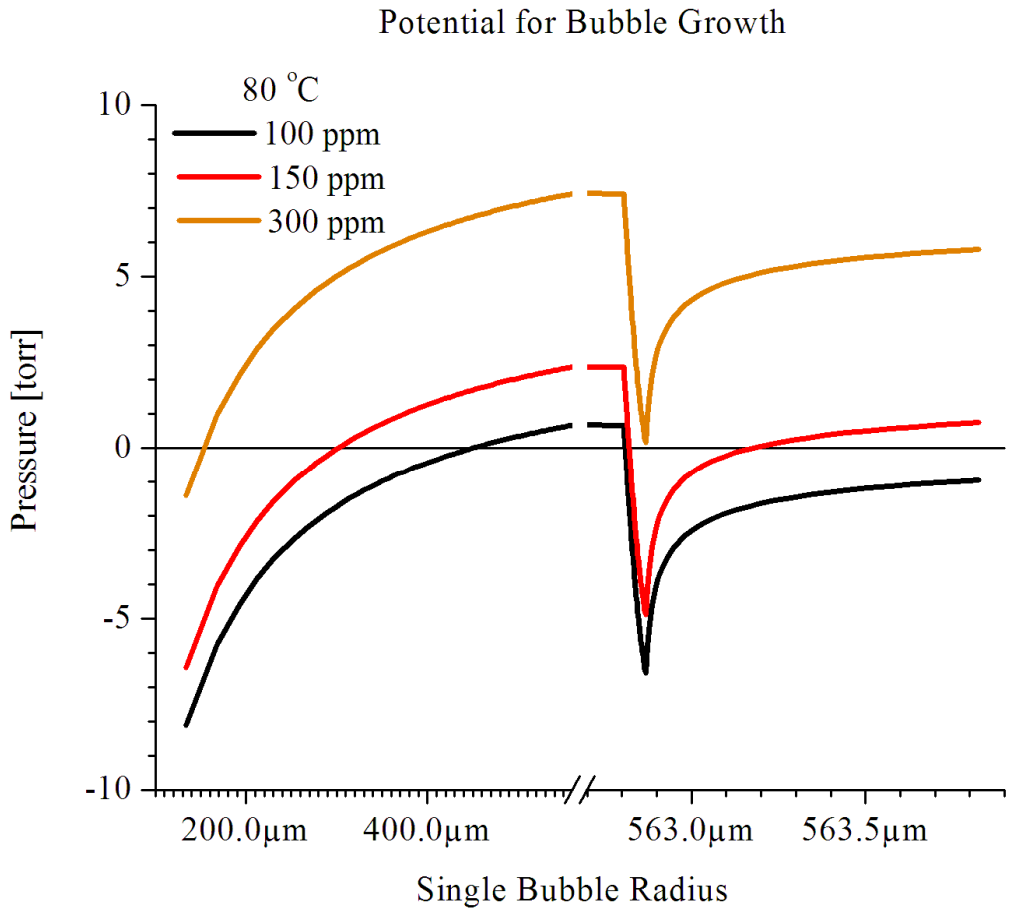

Figure 14. Potential for bubble growth expressed as a difference in equilibrium pressures (vapor pressure – bubble surface tension pressure – emitter meniscus pressure) vs. bubble radius for several concentrations of water in EMI–Im at 80 °C.

Multiple bubbles may also form, but their potentials for growth would be below the single bubble case shown here because for a given volume of extruded propellant, they would have smaller radii and thus greater surface tensions at the bubble walls. Thus, these plots give an indication of the minimum and maximum bubble radii that can be achieved by bubbles that may form in the bulk propellant. These restrictions do not apply to preexisting bubbles.

III. Conclusion

The current requirement for an upper limit of water in EMI–Im propellant is 150 ppm. It is recommended that this requirement stand. Further work may refine this requirement, but should lead to a higher confidence nonetheless. Future work includes measurement of the contact angle made between EMI–Im and emitter materials and calculations regarding optimization of the surface area and volume of the propellant manifold with respect to introduced water contamination.

Acknowledgments

The research work described in this paper was carried out at the Jet Propulsion Laboratory, California Institute of Technology, under a contract with the National Aeronautics and Space Administration. Reference herein to any specific commercial product, process, or service by trade name, trademark, manufacturer, or otherwise, does not constitute or imply its endorsement by the United States Government or the Jet Propulsion Laboratory, California Institute of Technology.

References

[1]Y-H Chiu,G Gaeta, D J Levandier, R A Dressler, J A Boatz, "Vacuum electrospray ionization study of the ionic liquid, [Emim][Im]," Journal of Mass Spectrometry, Vol. 265, 2007, pp. 146–158.

[2]R Kato, J Gmehling, "Measurement and correlation of vapor-liquid equilibria of binary systems containing the ionic liquids [EMIM][(CF3SO2)2N],[BMIM][(CF3SO2)2N], [MMIM][(CH3)2PO4] and oxygenated organic compounds respectively water," Fluid Phase Equilibria, Vol. 231, 2005, pp. 38–43

[3]M Krummen, P Wasserscheid, J Gmehling, "Measurement of Activity Coefficients at Infinite Dilution in Ionic Liquids Using the Dilutor Technique," Journal of Chemical and Engineering Data, Vol. 47, No. 6, 2002, pp. 1411–1417

[4]D S Abrams, J M Prausnitz, "Statistical thermodynamics of liquid mixtures: a new expression for the excess Gibbs energy of partly or completely miscible substances, AIChE J. 21 (1975) 116–128.

[5]P Kilaru, G A Baker, P Scovazzo, "Density and Surface Tension Measurements of Imidazolium-, Quaternary Phosphonium-, and Ammonium-Based Room-Temperature Ionic Liquids: Data and Correlations," Journal of Chemical and Engineering Data, Vol. 52, No. 6, 2007, pp. 2306–2314

[6]R C Weast, D R Lide, "CRC Handbook of Chemistry and Physics," 70th Edition, CRC Press, Inc, Bocan Raton, Florida, USA

[7]"User Guide for Models and Physical Properties," Version 3.4, Infochem Computer Services Ltd, London, England